Random-exchange Heisenberg behavior in the electron-doped quasi-one-dimensional spin-1 chain compound $AgVP_2S_6$

Peter T. Orban,[1,*] Shannon M. Bernier,[2] Tanya Berry,[1,2] Maxime A. Siegler,[2] and Tyrel M. McQueen[1,2,3,†]

[1]*Institute for Quantum Matter, William H. Miller III Department of Physics and Astronomy, The Johns Hopkins University, Baltimore, Maryland 21218, USA*

[2]*Department of Chemistry, The Johns Hopkins University, Baltimore, Maryland 21218, USA*

[3]*Department of Materials Science and Engineering, The Johns Hopkins University, Baltimore, Maryland 21218, USA*

(Received 25 March 2024; revised 1 July 2024; accepted 1 August 2024; published 14 August 2024)

Recent theoretical work suggests that a pair-density wave superconducting state can be realized by doping a one-dimensional spin-1 chain. Here, we report the physical properties of single crystals of $Mg_xAg_{1-x}VP_2S_6$ [$x = 0$, $x = 0.017(6)$, $x = 0.067(8)$, and $0.098(11)$] prepared by solid-state synthesis. Single-crystal x-ray-diffraction measurements confirm that Mg^{2+} is substituting for Ag^{+} to electron dope the V^{3+} zigzag chains. Magnetization measurements reveal that electron doping breaks up the V^{3+} chains, resulting in unpaired spins at the chain ends. The $Mg_xAg_{1-x}VP_2S_6$ series is consistent with random-exchange Heisenberg antiferromagnetic chain behavior and can be well described by the exchange-coupled pair model at low temperatures. Transport measurements show $Mg_xAg_{1-x}VP_2S_6$ remains insulating in the range $0 \leqslant x \leqslant 0.098(11)$, with the band gap decreasing to ~ 0.2 eV at $x = 0.098(11)$.

DOI: 10.1103/PhysRevB.110.054423

I. INTRODUCTION

Quantum magnetism remains an active research area in condensed-matter physics [1]. Magnetic ions interact with each other by exchange interactions, which results in different phases of matter including ordered phases like ferro- and antiferromagnetism, as well as various disordered phases. In certain crystal structures, magnetic ions are arranged in layers or chains, where interactions between layers or chains are small, making these effectively 2D or 1D magnetic materials. In lower dimensionalities, quantum fluctuations are enhanced, resulting in interesting quantum states of matter [2]. For example, the high-temperature cuprate superconductors originate from doping a spin-1/2 charge-transfer insulator with antiferromagnetic interactions in the 2D Cu-O plane [3]. In the 1D case, the gapped Haldane phase is realized in integer spin chains [4].

Depending on the interactions which are determined by the crystal structure, there can be a continuum between 2D and 1D magnetism. This system can be characterized by the Hamiltonian [5]

$$H = J\sum_i \left(S_i^x S_{i+1}^x + S_i^y S_{i+1}^y + \lambda S_i^z S_{i+1}^z\right) + J'\sum_{i,k} S_i S_k + D\sum_i S_i^z , \quad (1)$$

where J is the intrachain coupling constant, J' is the interchain coupling constant, λ is an exchange anisotropy parameter, D is single-ion anisotropy, and S_i^α are spin operators. When $|J'/J|$ becomes small, these systems can be considered as 1D spin chains. These systems are of theoretical interest due to the ability to test exactly solvable 1D models as well as the Haldane conjecture, which states that half-integer spin chains, such as $CuGeO_3$ [6], have gapless excitations whereas integer spin chains are gapped [7,8]. Low-dimensional quantum magnets also have potentially useful applications in 2D devices [9].

An exciting class of low-dimensional materials are the metal thiophosphates (MTPs), which have the general composition of $M_2^{2+}[P_2S_6]^{4-}$ (M = Fe, Mn, Ni, or other metals) where there are 2D layers of the M^{2+} cation. It is also possible to have an M^{+} and an M^{3+} cation, resulting in the general formula $(M^{1+}M^{3+})[P_2S_6]^{4-}$. The relative ionic radii of the M^{1+} and M^{3+} ions can tune these systems between 2D and 1D magnetism. For example, a large M^{1+} ion and a small M^{3+} ion results in widely separated chains of M^{3+}, making this a 1D material. MTPs have promising applications in 2D electronics because of their wide band-gap semiconducting properties as well as ferroelectric and magnetic properties [9–13]. They are also interesting from a fundamentals perspective since, depending on the transition metal, MTPs exhibit antiferromagnetism [14], spin glassiness [15], or more exotic phases such as the Haldane phase [4]. Furthermore, experimental studies on the MTP compound $FePS_3$ in the 2D limit show that antiferromagnetism is robust down to the monolayer [16,17].

Recent calculations by Zhang *et al.* suggest that a pair-density wave superconducting phase can be observed from hole doping a quasi-1D spin-1 Haldane chain [18]. Several quasi-1D spin-1 quantum magnets have been discovered, including $AgVP_2S_6$ [19], NDMAP [20], NENB [21], NENP [22], NINO [23], $PbNi_2V_2O_8$ [24], TMNIN

*Contact author: porban1@jhu.edu
†Contact author: mcqueen@jhu.edu

[25], and Y_2BaNiO_5 [26]. The MTP compound $AgVP_2S_6$ has very weak interchain interactions, $|J'/J| \sim 10^{-5}$, making this an effective experimental platform for studying the physics of spin-1 antiferromagnetic chains in 1D [4]. $AgVP_2S_6$ crystallizes in the monoclinic space group $P2/c$ (No. 13), with lattice parameters $a = 6.755$ Å, b 10.684 Å, $c = 5.921$ Å, and $\beta = 106.62°$ [27]. The structure follows *ABC* stacking, with a sulfur layer, a cation layer with Ag^+ and V^{3+}, followed by another sulfur layer. The cation plane is formed by alternating zigzag chains of Ag^+ and V^{3+} [shown in Fig. 1(a)], where the V^{3+} chain is formed by edge-sharing V-S octahedra and is antiferromagnetic [27]. The P-P dimers lie on the octahedral sites between the Ag^+ and V^{3+} chains, where each P atom is tetrahedrally coordinated with one P atom and three S atoms, and each S atom is bonded with P and coordinated by V^{3+} and Ag^+ sites [9]. The ground state of these systems is best pictured by the Affleck-Kennedy-Lieb-Tasaki (AKLT) state, where singlets form between V^{3+} sites as seen in Fig. 1(b) [28]. The Haldane gap has been confirmed by inelastic neutron-scattering experiments, and at low temperatures this system is proposed to be a random-exchange Heisenberg antiferromagnetic chain [4,29]. As seen in many high-temperature superconductors, the phenomena often emerge upon doping, so here we study the effects of doping on this 1D spin-1 system. Observing superconductivity in this system would be exciting, since few quasi-1D superconductors, such as $K_2Cr_3As_3$ [30] or the Bechgaard salts [31], exist mainly due to Peierls instability [32,33].

To explore this idea, we report the synthesis and physical properties of Mg-doped $AgVP_2S_6$. Analogous to how the high-temperature superconductors are doped adjacent to the Cu-O planes to make charge reservoirs, we substituted off the antiferromagnetic vanadium chain on the Ag^+ site, as opposed to directly on the vanadium chain. We successfully synthesized $Mg_xAg_{1-x}VP_2S_6$ for $x = 0$, $x = 0.017(6)$, $x = 0.067(8)$, and $x = 0.098(11)$, corresponding to electron doping. Attempts to further increase doping levels were unsuccessful. Rather than exhibiting superconductivity, the doped compound behaves as a random-exchange Heisenberg antiferromagnetic chain, which is well described by the exchange-coupled pair model. This is seen in the scaling of magnetic susceptibility as a function of temperature ($\chi \propto T^{-\alpha}$) and the magnetization as a function of magnetic field ($M \propto H^{1-\alpha}$).

II. METHODS

Stoichiometric amounts of Mg (Alfa Aesar, 99.8%), Ag (Alfa Aesar, 99.9%), V (Alfa Aesar, 99.5%), P (Sigma-Aldrich, 97%, purified using the technique outlined in Ref. [34]), and S (Thermo Scientific, 99.999%) powders were mixed with a mortar and pestle, then loaded into a quartz tube and sealed under vacuum at $\leqslant 2.5 \times 10^{-2}$ Torr. We targeted the nominal compositions $Mg_xAg_{1-x}VP_2S_6$, where $x = 0$, $x = 0.05$, $x = 0.10$, and $x = 0.15$. The ampoules were loaded into a box furnace and then heated to 600°C ($x = 0$), 638°C ($x = 0.05$), 625°C ($x = 0.10$), and 613°C ($x = 0.15$) at 50°C per hour and left to dwell for 72 h. After cooling to room temperature at 40°C per hour, the ampoules were removed from the furnace and opened, and single crystals in the form of small, black, needlelike flakes were picked out of the product.

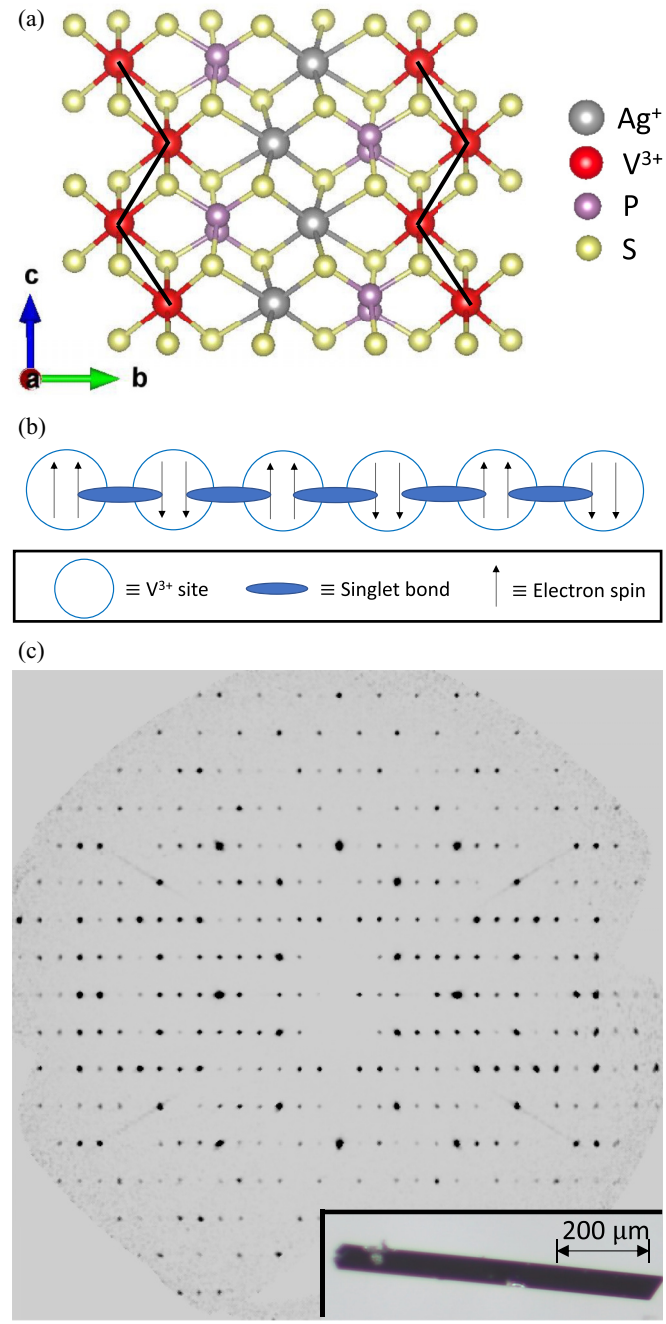

FIG. 1. (a) The crystal structure of $AgVP_2S_6$: there are alternating zigzag chains of magnetic V^{3+} ions and nonmagnetic Ag^+ ions in the *bc* plane. Solid lines are drawn to emphasize the zigzag V^{3+} chains. (b) The Affleck-Kennedy-Lieb-Tasaki (AKLT) state illustrates the ground state of a spin-1 Haldane chain. (c) Diffraction pattern of $(0kl)$ reflections for $AgVP_2S_6$ and picture of a $AgVP_2S_6$ crystal.

To determine the crystal structure and the amount of Mg substitution, single-crystal x-ray-diffraction (scXRD) data were collected at 213(2) K using a SuperNova diffractometer (equipped with an Atlas detector) with Mo Kα radiation ($\lambda = 0.710\ 73$ Å) with the program CRYSALISPRO (Version

CRYSALISPRO 1.171.42.49, Rigaku OD, 2022). The same program was used to refine the cell dimensions and for data reduction. The crystal structures were then solved using direct methods and refined using SHELXL [35] and WINGX [36]. Analytical numeric absorption correction using a multifaceted crystal model was applied using CRYSALISPRO as well as an empirical absorption correction using spherical harmonics, implemented in SCALE3 ABSPACK scaling algorithm [37]. The temperature of the data collection was controlled using the system Cryojet (manufactured by Oxford Instruments). A Hamilton R-test was also performed to estimate the uncertainty for the Mg occupancies [38] (see the Supplemental Material for details [39]).

A Quantum Design MPMS3 system was used to investigate the magnetic properties of the $Mg_xAg_{1-x}VP_2S_6$ series. Magnetization versus field at $T = 2$ K from $\mu_0 H = 0$–7 T and magnetic susceptibility versus temperature from $T =$ 2–300 K with an applied field of $\mu_0 H = 0.5$ T were measured for the entire series. Note that the magnetic susceptibility is approximated as the magnetization divided by the applied magnetic field ($\chi \approx M/H$). To mount the samples, a 3-mm $\times$ 3-mm $\times$ 0.5-mm quartz block with a thin layer of Apiezon N grease was used. We measured the magnetization as a function of temperature and field of the quartz block and N grease to subtract out the background. Dozens of crystals were lined up on the block, and these measurements were repeated for both parallel and perpendicular to the chain axis in the *bc* plane. Measurements perpendicular to the *bc* plane were not performed due to the large demagnetization factor in this geometry. Constant-temperature independent offsets were observed in repeated measurements on samples, so we applied a constant offset to match the susceptibilities at $T = 300$ K.

A Keithley 6517A high-resistance electrometer was used to investigate the transport properties of the $Mg_xAg_{1-x}VP_2S_6$ series using the two-probe force-voltage measure-current method. Samples were placed in a Quantum Design Physical Properties Measurement System for temperature control with the electrometer connected to the probe head via a custom breakout box. Resistance versus temperature measurements along the spin chain axis were performed with an applied voltage of 1.5 V for the parent compound and 3 V for the Mg-doped compounds.

III. RESULTS AND DISCUSSION

A. Single-crystal XRD

Crystal structure refinements for each composition were carried out while varying the Mg content (see Supplemental Material, SM) [39]. This is an effective way to find the Mg content due to the large difference in size and therefore charge density of Mg^{2+} and Ag^{+} ions. The actual Mg content was determined by tracking the R_1 statistic as a function of the Mg occupancy, which is a measure of the difference between calculated ($|F_c^{hkl}|$) and observed ($|F_o^{hkl}|$) structure-factor amplitudes. Plots of an R_1 statistic as a function of Mg occupancy are shown in Supplemental Material, Fig. S1, and the crystal structure and refinement parameters are summarized in SM, Table S2 [39]. The entire series crystallizes in the space group *P2/c* (13), and the Mg substitutes on the Ag site. The minimum of the R_1 statistic corresponds to the best estimate of Mg substitution. For the rest of this work, we will refer to the compounds based on the Mg content determined from the single-crystal XRD data as $x = 0$, $x = 0.017(6)$, $x = 0.067(8)$, and $x = 0.098(11)$ for the nominal compositions $x = 0$, $x = 0.05$, $x = 0.10$, and $x = 0.15$, respectively. This is estimated by using the 5% confidence level determined by the Hamilton-*R* test [38,39].

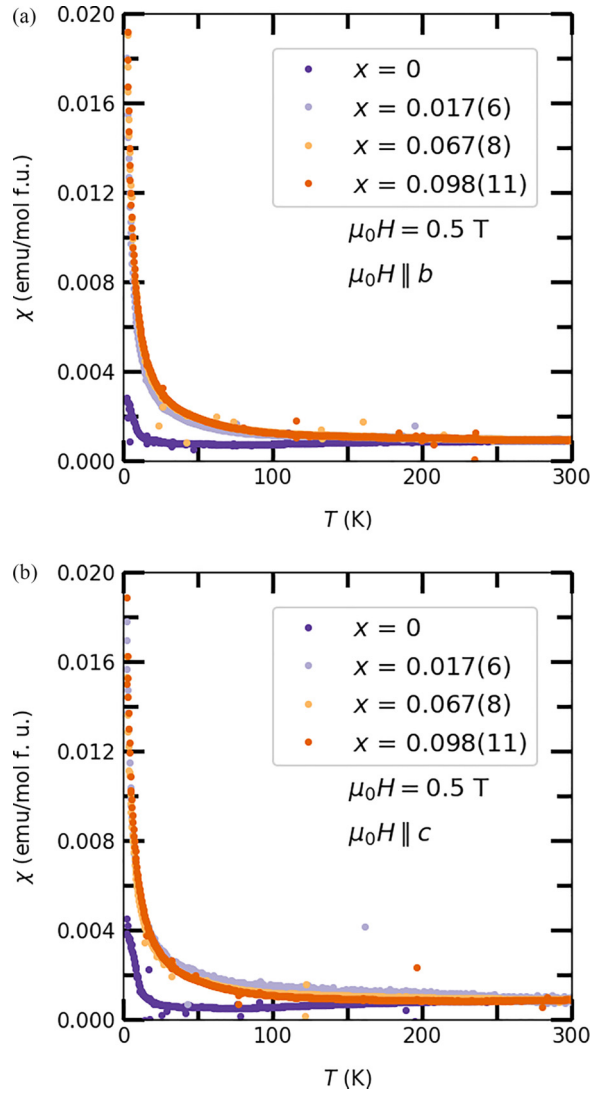

FIG. 2. Magnetic susceptibility vs temperature from $T = 2$–300 K for both (a) perpendicular ($\mu_0 H \parallel b$) and (b) parallel ($\mu_0 H \parallel c$) to the spin-chain axis where $\mu_0 H = 0.5$ T.

B. Magnetic characterization

Magnetic susceptibility as a function of temperature parallel and perpendicular to the chain axis in the *bc* plane is shown in Fig. 2. For the parent compound, we expect to see an $e^{-\Delta/T}/\sqrt{T}$ dependence because of the Haldane gap (Δ) [40]. At sufficiently low temperatures, the pairs of spin-1/2 spins on neighboring sites form a singlet state, leaving two unpaired spin-1/2 spins at the chain ends. The low-temperature upturn in the magnetic susceptibility is due to natural breaks in the

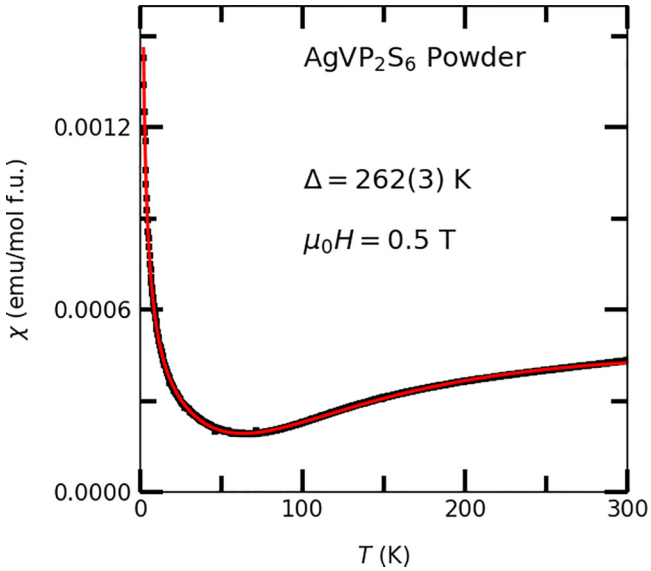

FIG. 3. Magnetic susceptibility vs temperature of a powder $AgVP_2S_6$ sample (black squares) fit to Eq. (2) (red line).

V^{3+} chains [29]. We can fit the χ vs T data to the model [41]

$$\chi(T) = \frac{A}{\sqrt{T}} e^{-(\Delta/k_B T)} + \frac{B}{T^{\alpha}} + \chi_0, \tag{2}$$

where the first term represents the contribution from Haldane-gapped spin-1 chains, the second term represents finite-segment interactions, and the last term is a constant diamagnetic offset. The fit for powder $AgVP_2S_6$ data shown in Fig. 3 yields a gap of $\Delta = 262(3)$ K, which is consistent with previous magnetic susceptibility measurements showing $\Delta = 250$ K [29]. According to theory, we can compute the intrachain coupling constant from $J = \Delta/0.41$, so $J = 640(7)$ K.

Upon doping, the power-law term remains dominant at low temperatures. This Curie-like term can be attributed to further chain breaks induced by the Mg^{2+} doping. Similar effects are seen in the magnetic susceptibility of $Y_2BaNi_{1-x}Zn_xO_5$, where nonmagnetic Zn^{2+} directly replaces spin-1 Ni^{2+} directly on the chain [42]. The parent compound $AgVP_2S_6$ can be explained as a random-exchange Heisenberg antiferromagnetic chain at low temperatures, which is described by the exchange-coupled pair model [29,43]. In this model, spins randomly occupy equally spaced sites with a probability p, resulting in dilute spins separated by nonmagnetic chains. Between the spins, there is a probability of exchange given by

$$P(J) = AJ^{-\alpha}, \tag{3}$$

where J decays exponentially with distance between the spins. As an approximation, the exchange between every other site is set to zero, so there is only an exchange interaction within pairs. The energy levels of each pair are the well-known singlet-triplet states, and therefore thermodynamic quantities can be easily computed [43].

In the low-temperature, low-field limit ($k_BT \ll J, E_{\text{Zeeman}} \ll k_BT$), the magnetic susceptibility is well described as a power law proportional to $T^{-\alpha}$, where $0.58 \leqslant \alpha \leqslant 0.87$, which is experimentally observed in other quasi-1D spin systems [41,43]. To investigate this across the series, we fit the low-temperature ($T < 50$ K) magnetic susceptibility to a power law:

$$\chi(T) = \frac{A}{T^{\alpha}} + \chi_0, \tag{4}$$

where α is the power-law exponent, A is a scale factor, and χ_0 is a diamagnetic offset (see SM for justification of this range selection [39]). Plots of the normalized magnetic susceptibility $(\chi - \chi_0)/A$ versus $T^{-\alpha}$ are shown in Fig. 4, and the fitting parameters are shown in SM, Table S7 [39].

For the parent compound, we find that $\alpha = 0.641(2)$, which is in excellent agreement with the literature [29]. With increased Mg^{2+} doping, we would naively expect more chain ends and α should approach 1, given that a system of free paramagnetic spins is described by the Curie law $\chi(T) \propto 1/T$. Initially, α increases upon doping with Mg. However, α decreases from $x = 0.017(6)$ to $x = 0.098(11)$ for both the fields parallel and perpendicular to the chain-axis configuration as seen in Fig. 5. As Mg^{2+} doping increases, there is a higher density of chain ends, and the average distance between chain ends decreases. The downward trend, or absence of a trend, in α could possibly be described by stronger interactions between the chain ends as the average chain length decreases. In addition, it appears that the perpendicular measurements have an α that is consistently higher in magnitude.

The single-crystal XRD data suggest that the Mg^{2+} is substituting on the Ag^{+} site, so these induced chain breaks from doping are likely V^{2+} ions, accounting for charge balance when replacing Ag^{+} with Mg^{2+}. Another possibility is the introduction of V vacancies for charge balance. Previous work on vanadium thiophosphate compounds suggest that V will readily change oxidation states given the existence of VPS_3 and the mixed-valence $V_{0.78}PS_3$ compounds [44–46]. In MTP compounds, it is also possible for metal vacancies to occur when intercalated with a charged species to charge balance [47–50]. To check for this possibility, we conduct scXRD refinements varying the V occupancy to check that the V content is consistent across the series (see Supplemental Material) [39]. For the $x = 0$, $x = 0.017(6)$, and $x = 0.067(8)$ samples, vanadium occupancy is within statistical error of 1 for all compositions. For $x = 0.098(11)$, we observe some V vacancies, 0.964(8), which is consistent with vacancies observed in $V_{0.78}PS_3$. The V vacancies at higher doping levels may also help explain the nonmonotonic trend in α. The uniformity in V content in the $x = 0$, $x = 0.017(6)$, and $x = 0.067(8)$ samples supports the idea that the V chains are structurally unaffected upon Mg doping, and the charge balance is achieved by the V ions shifting oxidation states. We note that the V^{2+} impurity has nonzero spin, unlike doping nonmagnetic impurities directly on the spin chain. However, its spin is different than the spin-1 V^{3+}, corresponding to introduction of unpaired spins and therefore a break in the V^{3+} chains. The doped samples have a much larger magnitude for the susceptibility, which is consistent with the idea that unpaired spins on the ends of chains are primarily contributing to the magnetization for a 1D antiferromagnet.

To further investigate the chain ends, magnetization as a function of magnetic field at $T = 2$ K is shown parallel

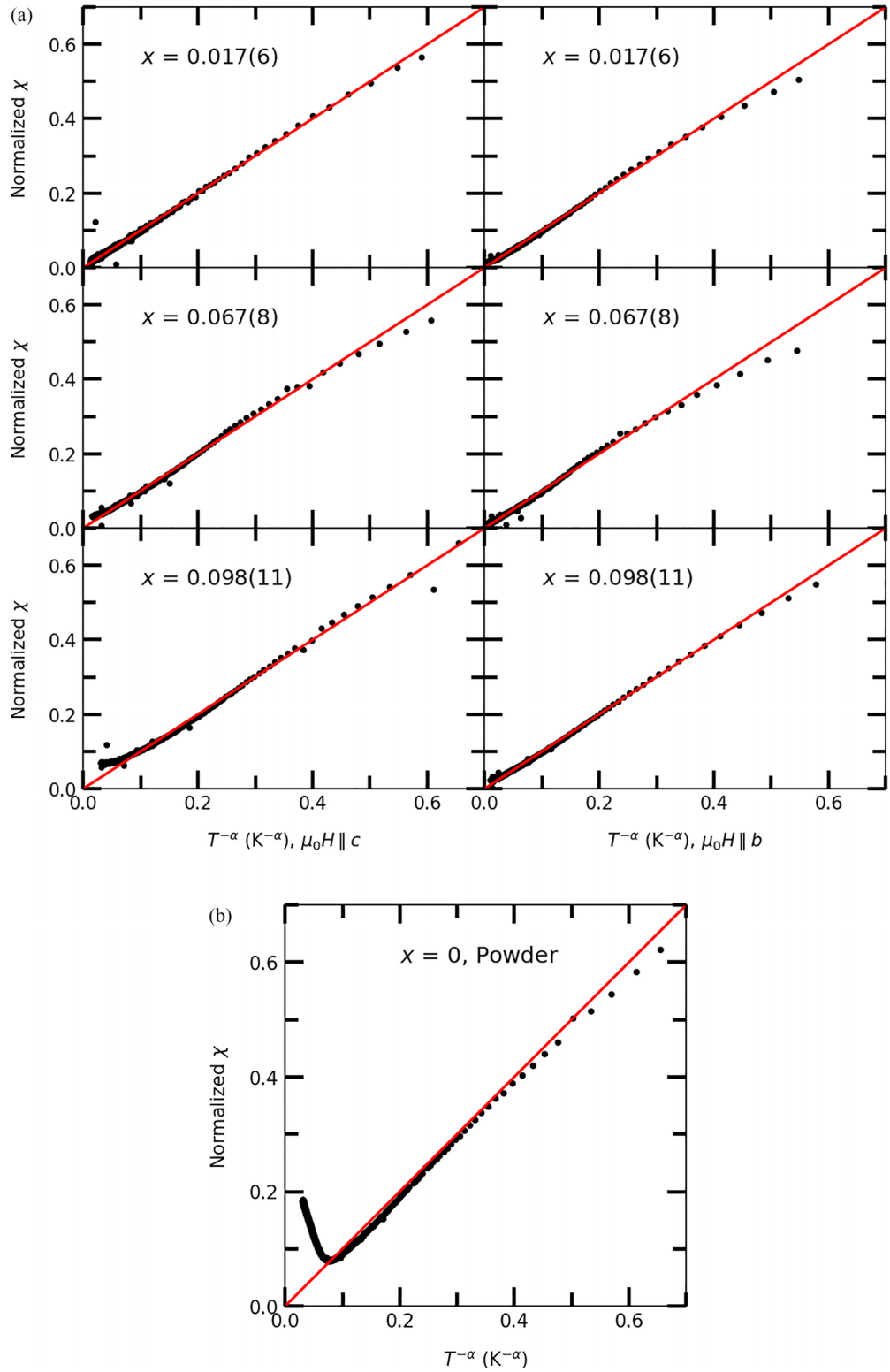

FIG. 4. Linearized plot of the normalized magnetic susceptibility $(\chi - \chi_0)/A$ vs $T^{-\alpha}$ for (a) $Mg_xAg_{1-x}VP_2S_6$ [$x = 0.017(6)$, 0.067(8), 0.098(11)] single-crystal samples and (b) a powder sample for the parent compound. The red line represents $(\chi - \chi_0)/A = T^{-\alpha}$.

and perpendicular to the chain axis in Fig. 6. There is not a clear trend in the magnitude of the magnetization as a function of doping. If we were doping on the V^{3+} chains with a nonmagnetic impurity, a monotonic increase in magnetization as a function of doping would be expected from the increased number of chain breaks and therefore unpaired spins. However, substituting Mg^{2+} on the Ag^{+} site introduces a V^{2+} impurity. These V^{2+} ions are still magnetic, and as a result can have greater or lesser magnetic interactions with the neighboring V^{3+} ions and further afield V^{2+} ions. In

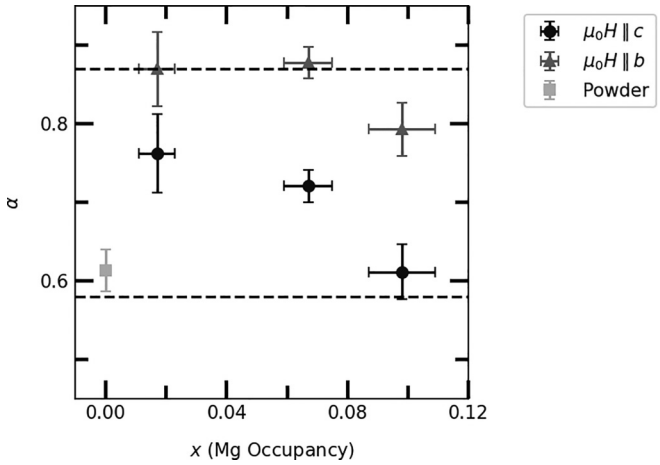

FIG. 5. Power-law exponent α as a function of Mg composition parallel ($\mu_0H \| c$) and perpendicular ($\mu_0H \| b$) to the chain axis as determined from magnetic susceptibility as a function of temperature measurements. The dashed line represents the limits of the range $0.58 \leqslant \alpha \leqslant 0.87$ as observed in 1D spin chains.

addition, the magnetization of the chain will depend upon the chain length as well, that is, if the chain has an even or odd number of V^{3+} sites. At higher Mg content, we also observe V

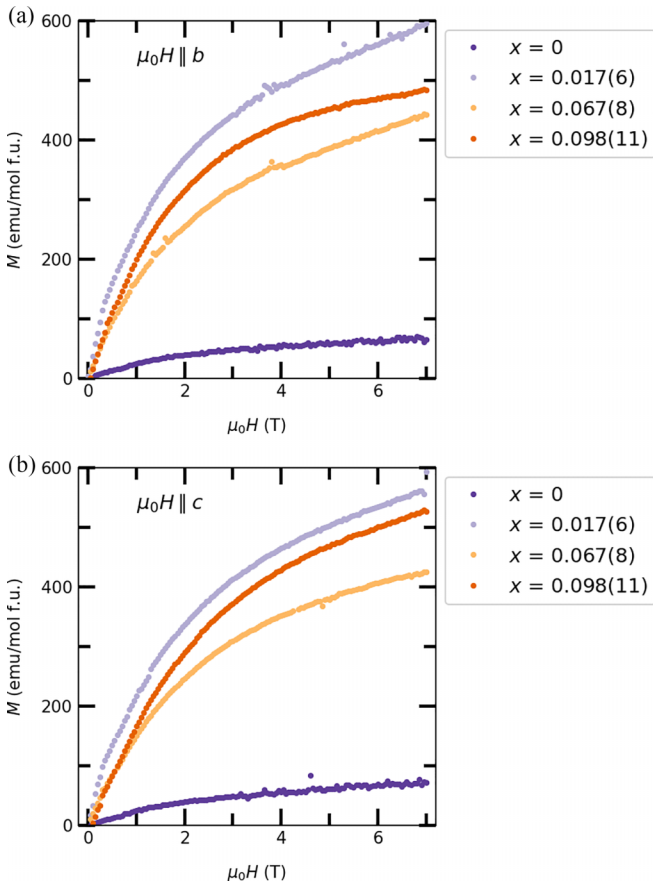

FIG. 6. Magnetization vs magnetic field at $T = 2$ K for $Mg_xAg_{1-x}VP_2S_6$ series with the magnetic field applied (a) perpendicular ($\mu_0H \| b$) and (b) parallel ($\mu_0H \| c$) to the chain axis.

vacancies. These factors provide natural explanations for the lack of a monotonic trend in the magnitude of magnetization, and we leave this question open for future studies. According to the exchange-coupled pair model, the magnetization as a function of magnetic field should scale as $M \propto H^{1-\alpha}$ in the intermediate-field regime $k_BT \ll g\mu_BH \ll J_0$, [42]. At $T = 2$ K, the lower limit of this range is roughly $\mu_0H = 1.5$ T, so the magnetization versus field curves are fit for $\mu_0H = 3$ T and above (see SM) [39]. The intrachain coupling constant of $J_0 = 640(7)$ K corresponds to a field of roughly 477 T, so fields up to 7 T are in the intermediate-field regime.

We fit the data to

$$M = C(\mu_0H)^{1-\alpha}, \tag{5}$$

where C is a scale factor and α is the same power-law exponent discussed previously, and the fit parameters are summarized in SM, Table S8 [39]. We plot M/C versus $(\mu_0H)^{1-\alpha}$ in Fig. 7 to show a linear trend at larger fields. As the magnetic field increases, the normalized magnetization converges to the expected scaling, suggesting that the exchange-coupled pair model is a valid description of Mg-doped $AgVP_2S_6$. The power-law exponent α as a function of Mg doping is also shown in Fig. 8. While there is not a clear trend, we see that α consistently agrees with the range 0.58 to 0.87, giving further evidence that this entire series is a random-exchange Heisenberg antiferromagnetic chain. We note that α measured from the isothermal magnetization measurements is consistently lower than the α determined from the magnetic susceptibility measurements. We attribute this to the different limiting cases examined, where the magnetic susceptibility tests the low-temperature, low-field limit and the isothermal magnetization measurements test the intermediate-field limit.

We now compare our results to other doped 1D spin chains in the literature. A classic example of a quasi-1D spin-1/2 chain is $CuGeO_3$, which undergoes a spin-Peierls transition at $T_{SP} = 14$ K [51,52]. The Cu^{2+} chain forms a 1D chain of spin-1/2 moments, and studies have been done of the effects of doping with both magnetic and nonmagnetic ions. Upon replacing Ge off chain with Si to make $CuGe_{1-x}Si_xO_3$, T_{SP} is suppressed and a Néel transition is observed at T_N, where $T_N < T_{SP}$, and T_{SP} disappears for higher levels of doping [53]. In the low-doping limit ($0.002 \leqslant x \leqslant 0.008$), Si doping frees three spin-1/2 spins for each Si impurity, and this is well described by a paramagnetic Curie-Weiss term between $T_N < T < T_{SP}$ [53]. In the higher-doping limit ($x \geqslant 0.05$), fitting a paramagnetic term $\chi_{para}(T) = C/T^{\alpha}$ with $\alpha < 1$ has been attempted without success [53]. Interestingly, the $\chi(T) = C/T^{\alpha}$ scaling behavior is observed when doping magnetic impurities (Fe^{2+}, Co^{2+}, Mn^{2+}) directly onto the Cu^{2+} chain, and the ground state of the Co- and Fe-doped compounds are described as a disorder-induced quantum critical Griffiths phase [54].

For quasi-1D spin-1 chains, experimental work has been done on doping the Haldane chain Y_2BaNiO_5 both on and off the Ni^{2+} chain. When replacing Y^{3+} with Ca^{2+} to make $Y_{2-x}Ca_xBaNiO_5$, spin-glass behavior is observed below $T = 3$ K [55]. Doping with nonmagnetic Zn^{2+} directly on the Ni^{2+} chains to make $Y_2BaNi_{1-x}Zn_xO_5$ effectively breaks Ni^{2+} chains into smaller segments [56]. Above $T = 4$ K, a model describing noninteracting segments of the chain

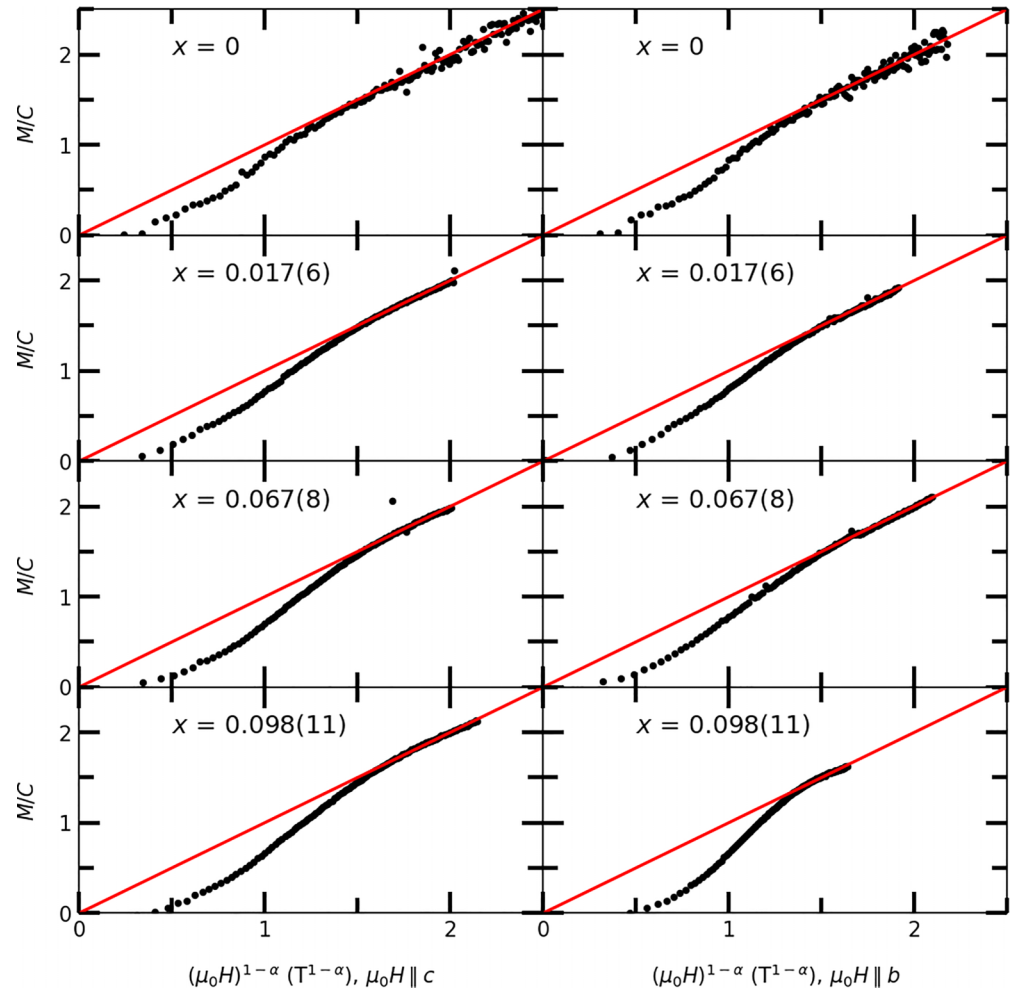

FIG. 7. Normalized magnetization M/C plotted against $(\mu_0 H)^{1-\alpha}$ for the $Mg_xAg_{1-x}VP_2S_6$ series. This model is valid for the intermediate-field limit, which is seen by M/C converging to $M/C = (\mu_0 H)^{1-\alpha}$ (red line) above a certain field.

captures the data well. However, below $T = 4$ K, there is a crossover to a sub-Curie regime, where for $\chi(T) = C/T^{\alpha}$, $\alpha = 0.83$, 0.79, and 0.76 for $x = 0.04$, 0.06, and 0.08, respectively [56], as well as $\alpha = 0.73$ for $Y_2BaNi_{1-x}Mg_xO_5$ [55]. These results are interpreted as the appearance of a gapless quantum phase due to a distribution of exchange couplings between dilution-induced moments, but the theoretical interpretation of the power-law scaling of the susceptibility remains open [56]. Due to the 1D nature of $AgVP_2S_6$, we believe $Mg_xAg_{1-x}VP_2S_6$ most closely resembles the parent compound with additional chain ends induced from the Mg doping, and based on our observations, it can be interpreted as a random-exchange Heisenberg antiferromagnetic chain. However, we leave the scaling of the susceptibility and magnetization of a doped quasi-1D spin-1 chain open for theoretical interpretation.

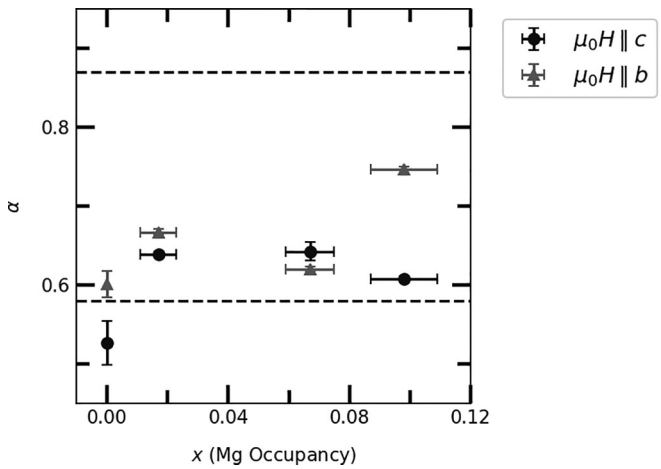

FIG. 8. Power-law exponent α as determined from magnetization vs field measurements at $T = 2$ K. The dashed line represents the limits of the range $0.58 \leqslant \alpha \leqslant 0.87$ observed experimentally for 1D spin chains.

C. Transport properties

Resistance as a function of temperature is shown in Fig. 9(a). Up to $x = 0.098(11)$, only insulating behavior is observed. In the intrinsic regime, the whole series shows thermally activated behavior described by

$$R(T) = R_0 e^{\Delta/2k_B T}, \tag{6}$$

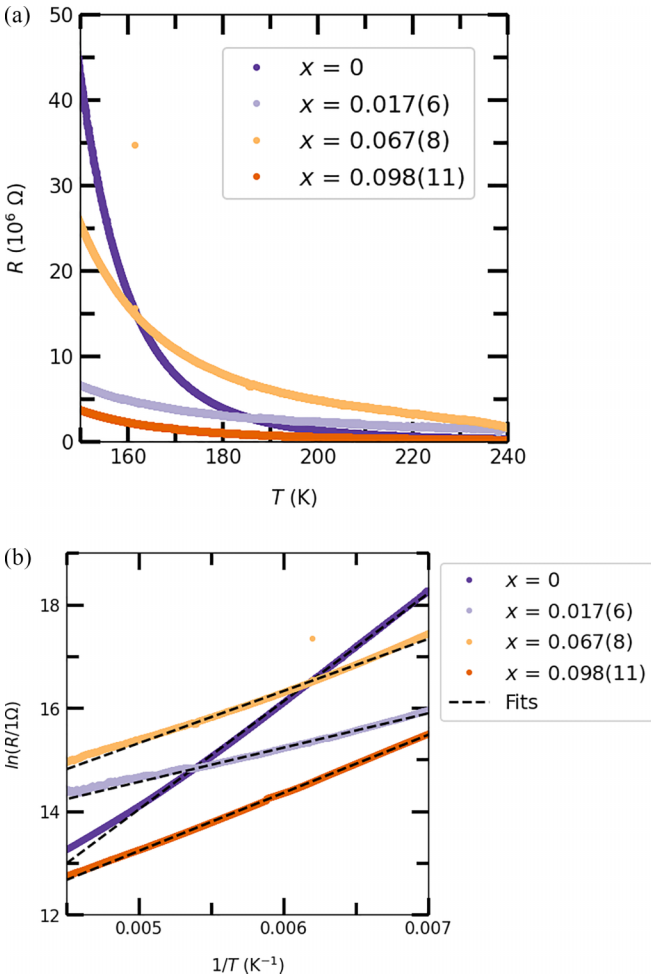

FIG. 9. (a) Resistance as a function of temperature for the $Mg_xAg_{1-x}VP_2S_6$ series. (b) Linearized plot of resistance as a function of temperature ($\ln R$ vs $1/T$) for the $Mg_xAg_{1-x}VP_2S_6$ series. The dashed line represents the fits used to determine the band gap.

where Δ is the band gap and R_0 is the infinite temperature resistance. The band gap can be estimated by plotting $\ln R$ vs $1/T$ and fitting the linear regime, as shown in Fig. 9(b). The band gap is then given by $\Delta = 2k_B m$, where m is the slope. The band gaps for each composition are summarized in Table I. Upon Mg^{2+} doping, the band gap is reduced by a factor of 2 with no clear trend, suggesting that Mg doping introduces a Mg impurity band that lies within the original gap. A monotonic trend may not occur here due to competition between the carrier concentration and scattering from impurities from Mg doping, and the V vacancies at higher Mg doping may also affect this.

TABLE I. Band gap determined from resistance measurements as a function of Mg occupancy.

x (Mg Occupancy)	Band gap (eV)
0	0.360(5)
0.017(6)	0.113(2)
0.067(8)	0.174(5)
0.098(11)	0.193(2)

IV. CONCLUSIONS

In conclusion, we present the synthesis of $Mg_xAg_{1-x}VP_2S_6$ as well as its magnetic and transport properties. Rather than producing a superconducting state, Mg^{2+} doping breaks the spin-1 chains into smaller segments. The low-temperature magnetism of the doped system can be described as random-exchange Heisenberg antiferromagnetic chains by the exchange-coupled pair model. In addition, a Mg^{2+} impurity band appears to be introduced which decreases the band gap by roughly half without the appearance of metallic behavior. In the future, one could explore hole doping a similar spin-1 system to see if superconductivity could be observed. This requires a deintercalation reaction to remove Ag from the system to form $Ag_{1-x}VP_2S_6$. Further studies about how the doping affects the magnetic ground state of the system may be interesting, and theoretical calculations concerning the effects of doping on the low-temperature thermodynamics of the system would also be insightful.

ACKNOWLEDGMENTS

This work was funded by the Institute for Quantum Matter, an Energy Frontier Research Center funded by the U.S. Department of Energy, Office of Science, Office of Basic Energy Sciences under Grant No. DE-SC0019331. The MPMS3 system used for magnetic characterization was funded by the National Science Foundation, Division of Materials Research, Major Research Instrumentation Program, under Award No. 1828490.

P.T.O. synthesized the materials and performed magnetic properties measurements under the supervision of T.M.M., P.T.O. collected the high-resistance data under the supervision of T.M.M., M.A.S. collected the single-crystal XRD data; P.T.O., S.M.B., T.B., and T.M.M. analyzed the data and interpreted the results; and P.T.O. and T.M.M. wrote the manuscript.

The authors declare that they have no competing interests.

[1] A. Vasiliev, O. Volkova, E. Zvereva, and M. Markina, Milestones of low-D quantum magnetism, npj Quant. Mater. **3**, 18 (2018).

[2] K. Wierschem and P. Sengupta, Characterizing the Haldane phase in quasi-one-dimensional spin-1 Heisenberg antiferromagnets, Mod. Phys. Lett. B **28**, 1430017 (2014).

[3] J. G. Bednorz and K. A. Miller, Possible high T_c superconductivity in the Ba-La-Cu-O System, Z. Phys. B **64**, 189 (1986).

[4] H. Mutka, J. L. Soubeyroux, G. Bourleaux, and P. Colombet, Support for the Haldane conjecture: Gap for magnetic excitations in the quasi-one-dimensional $S = 1$ Heisenberg antiferromagnet $AgVP_2S_6$, Phys. Rev. B **39**, 4820 (1989).

[5] C. Payen, P. Molinié, P. Colombet, and G. Fillion, Powder and single crystal susceptibility of the quasi-1D Heisenberg antiferromagnetic chain compounds $AgVP_2S_6$ ($S = 1$) and $AgCrP_2S_6$ ($S = 3/2$), J. Magn. Magn. Mater. **84**, 95 (1990).

[6] M. Hase, I. Terasaki, and K. Uchinokura, Observation of the spin-Peierls transition in linear Cu^{2+} (spin-1/2) chains in an inorganic compound $CuGeO_3$, Phys. Rev. Lett. **70**, 3651 (1993).

[7] H. A. Bethe, On the theory of metals. I. Eigenvalues and eigenfunctions of a linear chain of atoms, Z. Phys. **71**, 205 (1931).

[8] F. D. M. Haldane, Continuum dynamics of the 1-D Heisenberg antiferromagnet: Identification with the O(3) nonlinear sigma model, Phys. Lett. A **93**, 464 (1983); "Θ physics" and quantum spin chains (abstract), J. Appl. Phys. **57**, 3359 (1985).

[9] M. A. Susner, M. Chyasnavichyus, M. A. McGuire, P. Ganesh, and P. Maksymovych, Metal thio- and selenophosphates as multifunctional van der Waals layered materials, Adv. Mater. **29**, 1602852 (2017).

[10] R. Brec, D. M. Schleich, G. Ouvrard, A. Louisy, and J. Rouxel, Physical properties of lithium intercalation compounds of the layered transition chalcogenophosphates, Inorg. Chem. **18**, 1814 (1979).

[11] V. Maisonneuve, V. B. Cajipe, A. Simon, R. Von Der Muhll, and J. Ravez, Ferrielectric ordering in lamerallar $CuInP_2S_6$, Phys. Rev. B **56**, 10860 (1997).

[12] X. Bourdon, V. Maisonneuve, V. B. Cajipe, C. Payen, and J. E. Fischer, Copper sublattice ordering in layered $CuMP_2Se_6$, J. Alloys Compd. **283**, 122 (1999).

[13] V. Maisonneuve, C. Payen, and V. B. Cajipe, On $CuCrP_2S_6$: Copper disorder, stacking distortions, and magnetic ordering, J. Solid State Chem. **116**, 208 (1995).

[14] P. A. Joy and S. Vasudevan, Magnetism in the layered transition-metal thiophosphates MPS_3 (M = Mn, Fe, and Ni), Phys. Rev. B **46**, 5425 (1992).

[15] T. Masubuchi, H. Hoya, T. Watanabe, Y. Takahashi, S. Ban, N. Ohkubo, K. Takase, and Y. Takano, Phase diagram, magnetic properties and specific heat of $Mn_{1-x}Fe_xPS_3$, J. Alloys Compd. **460**, 668 (2008).

[16] J.-U. Lee, S. Lee, J. H. Ryoo, S. Kang, T. Y. Kim, P. Kim, C.-H. Park, J.-G. Park, and H. Cheong, Ising-type magnetic ordering in atomically thin $FePS_3$, Nano Lett. **16**, 7433 (2016).

[17] X. Wang, K. Du, Y. Y. F. Liu, P. Hu, J. Zhang, M. H. S. Owen, X. Liu, C. K. Gan, P. Sengupta, C. Kloc, and Q. Xiong, Raman spectroscopy of atomically thin two-dimensional magnetic iron phosphorus trisulfide ($FePS_3$) crystals, 2D Mater. **3**, 031009 (2016).

[18] Y.-H. Zhang and A. Vishwanath, Pair-density-wave superconductor from doping Haldane chain and rung-singlet ladder, Phys. Rev. B **106**, 045103 (2022).

[19] M. Takigawa, T. Asano, Y. Ajiro, M. Mekata, and Y. J. Uemura, Dynamics in the $S = 1$ one-dimensional antiferromagnet $AgVP_2S_6$ via ^{31}P and ^{51}V NMR, Phys. Rev. Lett. **76**, 2173 (1996).

[20] Z. Honda, K. Katsumata, Y. Nishiyama, and I. Harada, Field-induced long-range ordering in an $S = 1$ quasi-one-dimensional Heisenberg antiferromagnet, Phys. Rev. B **63**, 064420 (2001).

[21] E. Čižmar, M. Ozerov, O. Ignatchik, T. P. Papageorgiou, J. Wosnitza, S. A. Zvyagin, J. Krzystek, Z. Zhou, C. P. Landee, B. R. Landry, M. M. Turnbull, and J. L. Wikaira, Magnetic properties of the Haldane-gap material $[Ni(C_2H_8N_2)_2NO_2](BF_4)$, New J. Phys. **10**, 033008 (2008).

[22] I. A. Zaliznyak, D. C. Dender, C. Broholm, and D. H. Reich, Tuning the spin Hamiltonian of $Ni(C_2H_8N_2)_2NO_2ClO_4$, Phys. Rev. B **57**, 5200 (1998).

[23] J. P. Renard, M. Verdaguer, L. P. Regnault, W. A. C. Erkelens, J. Rossat-Mignod, J. Ribas, W. G. Stirling, and C. Vettier, Quantum energy gap in two quasi-one-dimensional $S = 1$ Heisenberg antiferromagnets, J. Appl. Phys. **63**, 3538 (1988).

[24] A. Zheludev, T. Masuda, I. Tsukada, Y. Uchiyama, K. Uchinokura, P. Böni, and S.-H. Lee, Magnetic excitations in coupled Haldane spin chains near the quantum critical point, Phys. Rev. B **62**, 8921 (2000).

[25] V. Gadet, M. Verdaguer, V. Briois, A. Gleizes, J. P. Renard, P. Beauvillain, C. Chappert, T. Goto, K. Le Dang, and P. Veillet, Structural and magnetic properties of $(CH_3)_4NNi(NO_2)_3$, Phys. Rev. B **44**, 705 (1991).

[26] J. Darriet and L. Regnault, The compound Y_2BaNiO_5: A new example of a Haldane gap in a $S = 1$ magnetic chain, Solid State Commun. **86**, 409 (1993).

[27] S. Lee, P. Colombet, G. Ouvrard, and R. Brec, A new chain compound of vanadium (III): $Ag_{12}V_{12}PS_3$ structure, metal ordering, and magnetic properties, Mater. Res. Bull. **21**, 917 (1986).

[28] I. Affleck, T. Kennedy, E. H. Lieb, and H. Tasaki, Rigorous results on valence-bond ground states in antiferromagnets, Phys. Rev. Lett. **59**, 799 (1987).

[29] H. Mutka, C. Payen, and P. Molinié, Finite segments, "free spins" and random exchange in spin $S = 1$ quasi one-dimensional antiferromagnets, Solid State Commun. **85**, 597 (1993).

[30] J.-K. Bao, J.-Y. Liu, C.-W. Ma, Z.-H. Meng, Z.-T. Tang, Y.-L. Sun, H.-F. Zhai, H. Jiang, H. Bai, C.-M. Feng, Z.-A. Xu, and G.-H. Cao, Superconductivity in quasi-one-dimensional $K_2Cr_3As_3$ with significant electron correlations, Phys. Rev. X **5**, 011013 (2015).

[31] K. Bechgaard and D. Jérome, Organic superconductors, Sci. Am. **247**, 52 (1982).

[32] S. van Smaalen, The Peierls transition in low-dimensional electronic crystals, Acta Crystallogr. Sect. A **61**, 51 (2005).

[33] R. E. Peierls, *Quantum Theory of Solids* (Oxford University, London, 1955).

[34] W. L. F. Armarego and C. L. L. Chai, *Purification of Laboratory Chemicals* (Elsevier, Amsterdam, 2009), p. 481.

[35] G. M. Sheldrick, Crystal structure refinement with *SHELXL*, Acta Crystallogr. Sect. C **71**, 3 (2015).

[36] L. J. Farrugia, *WinGX* suite for small-molecule single-crystal crystallography, J. of Appl. Crystallogr. **32**, 837 (1999).

[37] R. C. Clark and J. S. Reid, The analytical calculation of absorption in multifaceted crystals, Acta Crystallogr. Sect. A **51**, 887 (1995).

[38] W. C. Hamilton, Significance tests of the crystallographic R factor, Acta Crystallogr. **18**, 502 (1965).

[39] See Supplemental Material at http://link.aps.org/supplemental/10.1103/PhysRevB.110.054423 for single-crystal x-ray diffraction data and refinement details; the results and details of the Hamilton R test for both the Mg and V occupancy refinements; the fit parameter values and uncertainties for the magnetic susceptibility and isothermal magnetization data; and an analysis justifying the fit-range selection for the magnetic susceptibility and isothermal magnetization data.

[40] I. Affleck, Theory of Haldane-gap antiferromagnets in applied fields, Phys. Rev. B **41**, 6697 (1990).

[41] H. Mutka, C. Payen, and P. Molinie, Finite segments in quasi-1D Heisenberg antiferromagnets: Comparison of the isostructural systems $AgVP_2S_6$ ($S = 1$) and $AgCrP_2S_6$ ($S = 3/2$), J. Magn. Magn. Mater. **140**, 1677 (1995).

[42] J. Das, A. V. Mahajan, J. Bobroff, H. Alloul, F. Alet, and E. S. Sørensen, Comparison of $S = 0$ and $S = \frac{1}{2}$ impurities in the Haldane chain compound Y_2BaNiO_5, Phys. Rev. B **69**, 144404 (2004).

[43] W. G. Clark and L. C. Tippie, Exchange-coupled pair model for the random-exchange Heisenberg antiferromagnetic chain, Phys. Rev. B **20**, 2914 (1979).

[44] K. Ichimura and M. Sano, Valence states of layered vanadium chalcogenophosphates, Chem. Lett. **17**, 787 (1988).

[45] K. Ichimura, T. Miyazaki, S. Matsuzaki, and M. Sano, Electrical conductivities and electronic states of metal phosphorus trisulfides M_xPS_3 and their intercalation compounds, Mater. Sci. Forum. **91–93**, 505 (1992).

[46] G. Ouvrard, R. Fréour, R. Brec, and J. Rouxel, A mixed valence compound in the two dimensional MPS_3 family: $V_{0.78}PS_3$ structure and physical properties, Mater. Res. Bull. **20**, 1053 (1985).

[47] X. Zhang, H. Zhou, X. Su, X. Chen, C. Yang, J. Qin, and M. Inokuchi, Synthesis, characterization and magnetic properties of transition metal salen complexes intercalated into layered $MnPS_3$, J. Alloys Compd. **432**, 247 (2007).

[48] X. Chen, H. Zhou, L. Zou, C. Yang, J. Qin, and M. Inokuchi, A new organic-inorganic hybrid nanocomposite, BEDT-TTF intercalated into layered $FePS_3$, J. Incl. Phenom. Macrocycl. Chem. **53**, 205 (2005).

[49] A. A. El-Meligi, Synthesizing layered material of $FePS_3$ and its intercalation with pyridinum, Mater. Chem. Phys. **89**, 253 (2004).

[50] J. S. O. Evans, D. O'Hare, R. Clement, A. Leaustic, and P. Thuéry, Origins of the spontaneous magnetization in $MnPS_3$ Intercalates: A magnetic susceptibility and powder neutron diffraction study, Adv. Mater. **7**, 735 (1995).

[51] M. Hase, I. Terasaki, K. Uchinokura, M. Tokunaga, N. Miura, and H. Obara, Magnetic phase diagram of the spin-Peierls cuprate $CuGeO_3$, Phys. Rev. B **48**, 9616 (1993).

[52] K. Uchinokura, M. Hase, and Y. Sasago, Magnetic phase transitions in $CuGeO_3$ in high magnetic fields, Physica B **211**, 175 (1995).

[53] B. Grenier, J.-P. Renard, P. Veillet, C. Paulsen, R. Calemczuk, G. Dhalenne, and A. Revcolevschi, Magnetic susceptibility and phase diagram of $CuSe_{1-x}Si_xO_3$ single crystals, Phys. Rev. B **57**, 3444 (1998).

[54] S. V. Demishev, A. V. Semeno, and H. Ohta, Staggered field in quantum antiferromagnetic $S = \frac{1}{2}$ spin chain probed by high-frequency EPR (the Case of Doped $CuGeO_3$), Appl. Magn. Reson. **52**, 379 (2021).

[55] K. Kojima, A. Keren, L. P. Le, G. M. Luke, B. Nachumi, W. D. Wu, Y. J. Uemura, K. Kiyono, S. Miyasaka, H. Takagi, and S. Uchida, Muon spin relaxation and magnetic susceptibility measurements in the Haldane system $(Y_{2-x}Ca_x)Ba(Mi_{1-y}Mg_y)O_5$, Phys. Rev. Lett. **74**, 3471 (1995).

[56] C. Payen, E. Janod, and K. Schoumacker, C. D. Batista, K. Hallberg, and A. A. Aligia, Evidence of quantum criticality in the doped Haldane system Y_2BaNiO_5, Phys. Rev. B **62**, 2998 (2000).